


Evolution of the ionic polarization in multiple sequential ionization: General equations and an illustrative example

Elena V. Gryzlova ^{1,*} Maksim D. Kiselev ^{1,2,3} Maria M. Popova ^{1,2} and Alexei N. Grum-Grzhimailo¹

¹*Skobel'syn Institute of Nuclear Physics, Lomonosov Moscow State University, 119991 Moscow, Russia*

²*Faculty of Physics, Lomonosov Moscow State University, 119991 Moscow, Russia*

³*Laboratory for Modeling of Quantum Processes, Pacific National University, 680035 Khabarovsk, Russia*



(Received 26 July 2022; accepted 13 December 2022; published 23 January 2023)

Modern free-electron lasers generate a highly intense polarized radiation which initiates a sequence of ionization and decay events. Their probability depends on the polarization of each involved state as a function of time. Its complete account is limited by the fact that a state can be formed in various ways. Here we present an equivalent of rate equations for population that completely accounts for polarization of radiation formulated in terms of statistical tensors. To illustrate our approach we theoretically consider the sequential photoionization of krypton by an intense extreme ultraviolet femtosecond pulse for photon energies below the $3d$ -shell excitation threshold. The calculations of the ion yields, photoelectron spectra, and ionic polarization for various photon fluences are presented and the role of the polarization is discussed.

DOI: [10.1103/PhysRevA.107.013111](https://doi.org/10.1103/PhysRevA.107.013111)

I. INTRODUCTION

When an atom is irradiated by an intense electromagnetic field generated by a free-electron laser (FEL) operating in the extreme ultraviolet, the first photoionization act initiates a variety of competitive processes, such as sequential ionization, Auger decay, radiation decay, and others. The sample evolution depends on the radiation parameters: Intensity, pulse duration, and polarization [1,2]. The last is often left behind the scenes, in particular, because accounting for the polarization increases number of degrees of freedom enormously. The information about charge and state evolution of an irradiated sample is crucially important for a number of applications such as modeling the radioactive damage of biological samples for coherent diffraction imaging and as a fundamental test of the photoionization description basis [3,4].

Multiple ionization of atoms by FELs has been a subject of numerous and extensive investigations since the first observation at the free-electron laser in Hamburg FLASH [5]. Roughly multiple ionization may proceed in two regimes: (a) the strong-field regime involving multiphoton direct single or multiple ionization [6–8] and (b) the multiphoton sequential regime involving chains of subsequent ionization of different intermediate ion(s) with their possible excitation to discrete or autoionizing states [9–18]. Current research belongs to the second group. In general, both regimes may coexist and the question of whether to attribute a process to the first regime or to the second depends on the region of the considered photoelectron spectrum. It may be very tricky to distinguish the mechanisms based on ionic yields only [19,20]. Generally, the contribution of direct two-photon ionization tends to be lower in the x-ray regime [21].

One of the advantages of the FELs is that the generated radiation is highly polarized either linearly or circularly [22–24]. There is a variety of research devoted to an appearance of the polarization effects in the differential observable characteristics of sequential ionization: From photoelectron angular distribution [16,25–28] and angular correlation [15,29] up to the recent realization of *complete or perfect* experiment [17] or ion-ion correlation [8]. We are not aware of angle-resolved experiments proceeding with forming more than triple-charged ions [26,30].

On the other side, there has been much research on the polarization effects in integral cross sections mainly in an integral linear or circular dichroism within a pump-probe scheme [31–36]. Polarization of an ionized state may appear as a variation of ionization probability up to complete suppression. The dynamically quasiforbidden transitions in the photoionization of the pumped open-shell atoms were found and interpreted [37].

In spite of the fact that numerous investigations of dichroism have shown that polarization may affect integral characteristics such as ionic yield and the photoelectron spectrum, to the best of our knowledge, there are no studies investigating multiple ionization with complete accounting of intermediate states polarization. This type of research is quite resource consuming because it supposes to solve a system of the rate equations for all affected magnetic sublevels instead of having one equation for one state that increases the number of equations significantly [1,38]. Therefore, it is common to use relevant ionization and excitation cross sections by polarized radiation neglecting the influence of subsequenced steps to the former one which may cause the depletion of magnetic sublevels.

In the paper we develop a method suitable for an atom (ion) in linearly or circularly polarized radiation under assumption that the levels are separated, and therefore populated

*gryzlova@gmail.com

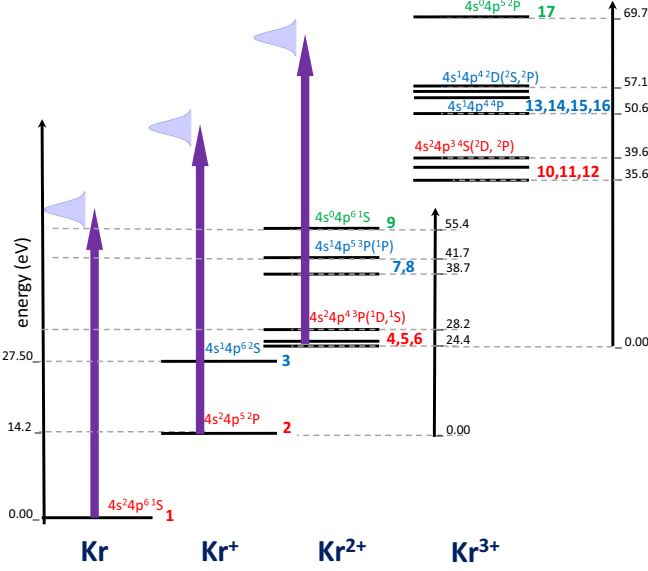
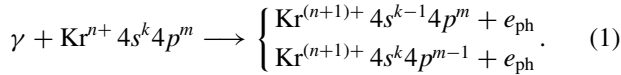


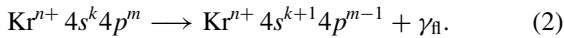
FIG. 1. The scheme of transitions in the sequential multiphoton ionization of Kr. The experimental ionization thresholds are taken from [52] and averaged over a multiplet.

incoherently. The method is based on solution of the system of equations for statistical tensors. The system is similar to the one for populations which is widely used in the description of atom-field interaction [39–47].

As an illustrative example we consider the sequential ionization of krypton by an electromagnetic pulse with photon energy 60–80 eV that is below the lowest excitation energy of the $3d$ shell ($3d^9 5p^1 P_1$, or more precisely $3d^9 5p[3/2]_1$, 91.2 eV [48]). For both single or double $4s$ -vacancy states the Auger decay is energetically forbidden, therefore the dominant process governing temporal dynamics is the subsequent photoionization from the $4s$ and the $4p$ orbitals with emission of a photoelectron e_{ph} :



Relaxation of the $4s$ vacancies proceeds via radiative transition from the $4p$ to the $4s$ level with fluorescence of a photon γ_{fl} :



We consider relatively short femtosecond pulses, therefore the relaxation transitions can be neglected. It is worth noting that, since a vacancy in the $4p$ shell is created, there is a possibility to excite resonance $3d^{10} 4s^2 4p^5 2P_{3/2,1/2} \rightarrow 3d^9 4s^2 4p^6 2D_{5/2,3/2}$, i.e., to observe *hidden resonance*, similar to one discussed in [10]. In order to evaluate its energy one can take experimental values of ionization potentials for the $4p$ and the $3d$ shells in neutral krypton from [49] ($4p_{3/2}$, 14 eV; $4p_{1/2}$, 14.67 eV; $3d_{5/2}$, 93.81 eV; $3d_{3/2}$, 95.05 eV). Then the averaged over fine-structure energy of the resonance is 80.1 eV.

The scheme of the sequential ionization from neutral Kr to the triply charged ion Kr^{3+} involving the $4s$ and $4p$ shells of Kr and its ions is shown in Fig. 1, where considered configura-

tions, terms, and relative energies are indicated. The additional details needed for interpretation of the photoelectron spectrum are presented in Table I. We neglect fine-structure splitting, do not include shakeup, direct two-photon and one-photon double ionization channels [50], and consider the sequential ionization up to triple three-photon ionization exactly in the same setup as we did in [51] for the *unpolarized* radiation.

For the sake of brevity in the paper we discuss the polarization effects observed in ionic yields of low charged (<3) ions and the photoelectron spectrum corresponding binding energy below 50 eV, which cannot be affected by possible ionization of Kr^{3+} and further.

In the next section we outline a theoretical approach for modeling the atom-field interaction based on the solution of a system of the rate equations for statistical tensors. In Sec. III, we present a thorough analysis of the ionic polarization. In Sec. IV, the results on the time evolution of the Kr target under the FEL pulse (ionic yields) and the resulting photoelectron spectra are presented and discussed. We use atomic units unless otherwise indicated.

II. THE SYSTEM OF EQUATIONS FOR EVOLUTION OF THE STATISTICAL TENSORS

The goal of this section is to formulate an equivalent of the rate equations accounting for polarization of the states in terms of the statistical tensors for linearly and circularly polarized radiation in the dipole approximation. Under these conditions, the statistical tensor of photons $\rho_{k_\gamma q_\gamma} \neq 0$ for $q_\gamma = 0$ and $k_\gamma \leq 2$. We leave treating of an electron-ionic correlation out, hence only zero rank statistical tensors of an electron $\rho_{k_e=0, q_e=0}$ exist. Therefore all nonzero statistical tensors of ionic states have projection $q = 0$.

It is well established [53,54] that if a state i of a n -charged ion A^{n+} with total angular momentum J_i absorbs a (dipole) photon and ionizes into a state f of $A^{(n+1)+}$ with total momentum J_f , the statistical tensors of the initial $\rho_{k_i 0}(J_i)$ and final $\rho_{k_f 0}(J_f)$ states are connected by the equation

$$\rho_{k_f 0}(J_f) = \sum_{k_\gamma} \rho_{k_i 0}(J_i) S[k_i, k_\gamma, k_f], \quad (3)$$

where transition parameter $S[k_i, k_\gamma, k_f]$ is presented in terms of the reduced ionization amplitudes as

$$\begin{aligned} S[k_i, k_\gamma, k_f] &= 4\pi^2 \alpha \omega \rho_{k_\gamma 0} B[k_i, k_\gamma, k_f], \quad (4) \\ B[k_i, k_\gamma, k_f] &= \hat{k}_i \hat{k}_\gamma (k_i 0, k_\gamma 0 | k_f 0) \frac{\hat{J}_f}{\hat{J}_i} (-1)^{J_f + k_f} \\ &\times \sum_{j J_j'} \hat{J}_j' (-1)^{J' + j} \begin{Bmatrix} J_f & J_f & k_f \\ J & J' & j \end{Bmatrix} \\ &\times \begin{Bmatrix} J_i & 1 & J \\ J_i & 1 & J \\ k_i & k_\gamma & k_f \end{Bmatrix} \\ &\times \langle (J_f j) J || \hat{D} || J_i \rangle \langle (J_f j) J' || \hat{D} || J_i \rangle^*. \quad (5) \end{aligned}$$

Here $\hat{a} = \sqrt{2a+1}$, \hat{D} is the operator of the atomic electric dipole momentum, and the usual notation for Clebsch-Gordan coefficients, $6j$ and $9j$ symbols, is used. Throughout the paper we use nonconventional normalization of the statistical ten-

TABLE I. The list of the pathways in the sequential three-photon ionization of Kr within the LS-coupling scheme. The columns and lines correspond to the initial and final states of the pathway, respectively. MR is the maximal rank feasible for a state at sequential ionization. We denote different transitions contributed to a one photoelectron line by a capital letter. Numbers are experimental ionization thresholds [52] for the corresponding transitions in eV, averaged over a multiplet. The unmarked transitions are weak and their contribution to the photoelectron spectra is negligible.

N	Final	N MR initial	1 $4s^24p^6\ ^1S$	2 $4s^24p^5\ ^2P^o$	3 $4s^14p^6\ ^2S$	4 $4s^24p^4\ ^3P$	5 $4s^24p^4\ ^1D$	6 $4s^24p^4\ ^1S$	7 $4s^14p^5\ ^3P^o$	8 $4s^14p^5\ ^1P^o$	9 $4s^04p^6\ ^1S$
1	$4s^24p^6\ ^1S$	0	—	—	—	—	—	—	—	—	—
2	$4s^24p^5\ ^2P^o$	2	A, 14.2	—	—	—	—	—	—	—	—
3	$4s^14p^6\ ^2S$	0	D, 27.5	—	—	—	—	—	—	—	—
4	$4s^24p^4\ ^3P$	2	—	B, 24.4	—	—	—	—	—	—	—
5	$4s^24p^4\ ^1D$	4	—	C, 26.0	—	—	—	—	—	—	—
6	$4s^24p^4\ ^1S$	0	—	E, 28.2	—	—	—	—	—	—	—
7	$4s^14p^5\ ^3P^o$	2	—	H, 38.7	C, 25.4	—	—	—	—	—	—
8	$4s^14p^5\ ^1P^o$	2	—	J, 41.7	E, 28.4	—	—	—	—	—	—
9	$4s^04p^6\ ^1S$	0	—	—	K, 42.1	—	—	—	—	—	—
10	$4s^24p^3\ ^4S^o$	0	—	—	—	F, 35.6	—	—	—	—	—
11	$4s^24p^3\ ^2D^o$	4	—	—	—	G, 37.8	F, 36.3	34.0	—	—	—
12	$4s^24p^3\ ^2P^o$	2	—	—	—	I, 39.6	G, 38.1	F, 35.8	—	—	—
13	$4s^14p^4\ ^4P$	2	—	—	—	50.6	—	—	F, 36.2	—	—
14	$4s^14p^4\ ^2D$	4	—	—	—	53.7	52.2	49.9	I, 39.4	F, 36.4	—
15	$4s^14p^4\ ^2S$	0	—	—	—	57.1	55.6	53.3	K, 42.8	I, 39.8	—
16	$4s^14p^4\ ^2P^b$	2	—	—	—	56.0	54.4	52.1	J, 41.6	H, 38.6	—
17	$4s^04p^5\ ^2P^{oa}$	2	—	—	—	—	—	—	55.4	52.4	H, 38.7

^aEnergy of this state is taken from [59].

^bIn NIST database sublevels relevant for this state are identified as $4s4p^4\ ^2P_{1/2}$ (20.6), $4s4p^4\ ^2P_{3/2}$ (25.46), $4s^24p^2\ ^3P\ 4d_{3/2}$ (20.26), and $4s^24p^2\ ^3P\ 4d_{1/2}$ (25.38). Our calculations have shown that the state with energy 20.26 eV should be interpreted as $4s4p^4\ ^2P_{3/2}$.

sors: if state J_a is completely populated, $\rho_{00}(J_a) = 1$ [instead $\rho_{00}(J_a) = 1/\hat{J}_a$] that allows us to consider zero rank statistical tensors as population in percents [summed over all states' population $\sum_a \rho_{00}(J_a) = 1$]. Parameter $S[0, 0, 0]$ is the ionization cross section of an unpolarized state with J_i to an ion with J_f .

The transparent way to obtain the time-dependent form of (3) is to start with conventional rate equations for the level populations:

$$\frac{dN_{aM_a}(t)}{dt} = j(t) \sum_{b \neq a, M_b}^L [\sigma_{bM_b \rightarrow aM_a} N_{bM_b}(t) - \sigma_{aM_a \rightarrow bM_b} N_{aM_a}(t)], \quad (6)$$

where $N_{aM_a}(t)$ is the population of sublevel a with magnetic quantum number M_a and $j(t)$ is the time-dependent intensity of the incident radiation (envelope), L is the number of the accounted for states, and $\sigma_{aM_a \rightarrow bM_b}$ is the photoionization cross section from sublevel aM_a of A^{n+} to sublevel bM_b of $A^{(n+1)+}$ which is connected with transition parameter (4):

$$\sigma_{iM_i \rightarrow fM_f} = \frac{\hat{J}_i}{\hat{J}_f} \sum_{k_i, k_\gamma, k_f} (-1)^{J_i - M_i + J_f - M_f} (J_i M_i, J_i - M_i | k_i 0) \times (J_f M_f, J_f - M_f | k_f 0) S[k_i, k_\gamma, k_f]. \quad (7)$$

The total ionization cross section of an unpolarized state by the unpolarized radiation is an averaged sum of cross

sections from magnetic sublevels:

$$\sigma = \frac{\sum_{M_i M_f} \sigma_{iM_i \rightarrow fM_f}}{2J_i + 1} \equiv S[0, 0, 0]. \quad (8)$$

The statistical tensor corresponding to a state a is constructed from its population $N_{aM_a}(t)$ straightforwardly by the definition

$$\rho_{k_a 0}(J_a) = \hat{J}_a \sum_{M_a} (-1)^{J_a - M_a} (J_a M_a, J_a - M_a | k_a 0) N_{aM_a}, \quad (9)$$

$$N_{aM_a} = \frac{1}{\hat{J}_a} \sum_{k_a} (-1)^{J_a - M_a} (J_a M_a, J_a - M_a | k_a 0) \rho_{k_a 0}(J_a). \quad (10)$$

Summarizing the above, we may write down the analog of the rate equations (6) in terms of statistical tensors:

$$\frac{d\rho_{k_a 0}(J_a)}{dt} = \frac{d\rho_{k_a 0}(J_a)}{dt} \Big|_{\text{in}} - \frac{d\rho_{k_a 0}(J_a)}{dt} \Big|_{\text{out}}, \quad (11)$$

where the term describing pumping of population ($b = i$ is initial, $a = f$ is final) is quite simple:

$$\begin{aligned}
\left. \frac{d\rho_{k_a 0}(J_a)}{dt} \right|_{\text{in}} &= j(t) \hat{J}_a \sum_{M_a b M_b} (-1)^{J_a - M_a} (J_a M_a, J_a - M_a | k_a 0) \sigma_{b M_b \rightarrow a M_a} N_{b M_b} \\
&= j(t) \sum_{\substack{M_a b M_b \\ k'_a k_\gamma k_b k'_b}} (J_a M_a, J_a - M_a | k_a 0) (J_a M_a, J_a - M_a | k'_a 0) (J_b M_b, J_b - M_b | k_b 0) (J_b M_b, J_b - M_b | k'_b 0) \\
&\quad \times S[k_b, k_\gamma, k'_a] \rho_{k_b 0}(J_b) = j(t) \sum_{k_\gamma b k_b} S[k_b, k_\gamma, k_a] \rho_{k_b 0}(J_b). \tag{12}
\end{aligned}$$

The term describing the leakage of population ($a = i$ is initial, $b = f$ is final) is much trickier:

$$\begin{aligned}
\left. \frac{d\rho_{k_a 0}(J_a)}{dt} \right|_{\text{out}} &= j(t) \hat{J}_a \sum_{M_a b M_b} (-1)^{J_a - M_a} (J_a M_a, J_a - M_a | k_a 0) \sigma_{a M_a \rightarrow b M_b} N_{a M_a} \\
&= j(t) \frac{\hat{J}_a}{\hat{J}_b} \sum_{\substack{M_a b M_b \\ k'_a k'_\gamma k_\gamma k_b}} (-1)^{J_a - M_a} (J_a M_a, J_a - M_a | k_a 0) (J_a M_a, J_a - M_a | k'_a 0) (J_a M_a, J_a - M_a | k'_a 0) \\
&\quad \times (-1)^{J_b - M_b} (J_b M_b, J_b - M_b | k_b 0) S[k'_a, k_\gamma, k_b] \rho_{k'_a 0}(J_a) \\
&= j(t) \hat{J}_a \sum_{k'_a k'_\gamma k_\gamma} (-1)^{k'_a} \hat{k}'_a(k_a 0, k'_a 0 | k'_a 0) \begin{Bmatrix} k_a & k'_a & k'_a \\ J_a & J_a & J_a \end{Bmatrix} S[k'_a, k_\gamma, 0] \rho_{k'_a 0}(J_a). \tag{13}
\end{aligned}$$

The feature of this equation is that, while in the rate equations for population a leakage of a population is always proportional to it, in the rate equations for the statistical tensors a leakage of a tensor depends on other tensors of the state. If one keeps in Eqs. (11)–(13) the terms with $k_\gamma = 0$ only that correspond to the *unpolarized* radiation, that automatically smears out all terms with $k_s \neq 0$ and vice versa. Thus, the unpolarized radiation and neglecting polarization of the ions are equivalent.

Having Eqs. (11)–(13), one can solve the system for the statistical tensors which is completely similar to the conventional rate equations apart from the specific form of the coefficients. The advantage of this approach is that with more states involved the size of system (11) increases slower than the size of system (6) where magnetic quantum numbers are directly accounted for. In the considered illustrative example (see Table I) $L = 17$, the number of magnetic sublevels is $\sum_a (2J_a + 1) = 45$, and the number of statistical tensors is 31.

Time-dependent alignment and orientation of an ion are the ratio of the corresponding statistical tensors:

$$A_2(J_f) = \frac{\rho_{20}(J_f)}{\rho_{00}(J_f)}, \quad A_1(J_f) = \frac{\rho_{10}(J_f)}{\rho_{00}(J_f)}. \tag{14}$$

For the forthcoming discussion let us introduce the conventional *stationary* alignment of a state f :

$$\mathcal{A}_f = \frac{-\sqrt{2}B[0, 2, 2] + \mathcal{A}_i(B[2, 0, 2] - \sqrt{2}B[2, 2, 2])}{B[0, 0, 0] - \sqrt{2}B[2, 2, 0]}. \tag{15}$$

By the *stationary* alignment we mean the alignment obtained in some branch $i \rightarrow f$ neglecting all other pathways as well as depletion or saturation of the considered state.

There are maximal and minimal values of an alignment directly following from the statistical tensor definition:

$$A_2(J) = \frac{\sum_M (-1)^{J_M} (JM, J - M | 20) N_{JM}}{\sum_M (-1)^{J_M} (JM, J - M | 00) N_{JM}}, \tag{16}$$

that gives

$$A_2(P) = \frac{1}{\sqrt{2}} \frac{N_{11} + N_{1-1} - 2N_{10}}{N_{11} + N_{1-1} + N_{10}}, \tag{17}$$

$$A_2(D) = \sqrt{\frac{10}{7}} \frac{N_{22} + N_{2-2} - (N_{21} + N_{2-1})/2 - N_{20}}{N_{22} + N_{2-2} + N_{21} + N_{2-1} + N_{10}}. \tag{18}$$

Apparently for the P -term states the maximal and minimal alignment are $1/\sqrt{2}$ and $-\sqrt{2}$, correspondingly (17); for the D term they are $\sqrt{10/7}$ and $-\sqrt{10/7}$ (18). It is important to note that the fourth rank (and higher if possible) tensors are not perturbation to the second rank tensors. Neglecting the fourth ranks may lead to an unphysical value of an alignment which means negative population of some magnetic sublevels.

The Gaussian distribution of the incident *photon flux density* is assumed:

$$j(t) = j_0 \exp(-t^2/t_p^2), \tag{19}$$

thus the pulse full width at half maximum (FWHM) is equal to $2\sqrt{\ln 2} t_p$. The integral number of photons per 1 \AA^2 in the entire pulse, i.e., *fluence* F , is related to the intensity as

$$j_0 = \frac{2\sqrt{\ln 2} F}{\sqrt{\pi} \text{FWHM}} = 0.0063634 \frac{F [\text{ph}/\text{\AA}^2]}{\text{FWHM} [\text{fs}]}. \tag{20}$$

The typical pulse duration obtained at the seeded FEL FERMI [55,56] is around 50–100 fs; we set the pulse duration to $t_p = 60$ fs (FWHM = 100 fs).

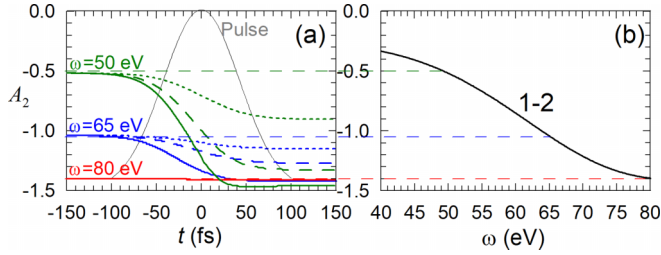


FIG. 2. (a) The alignment of the $\text{Kr}^+4s^2 4p^5 2P$ ion calculated as a function of time at $\omega = 50, 65,$ and 80 eV. The solid, dashed, and dotted lines correspond to fluence $F = 3000, 1000,$ and 400 ph/Å², respectively. (b) Conventional alignment of the same ion as a function of energy (accounting for the difference in definitions these data are in accordance with [58]). Here “1-2” and after “a-b” indicates the transition between the states labeled according to Table I.

III. ANALYSIS OF THE IONS ALIGNMENT

The photoionization cross sections of $4s^k 4p^m 2S+1L$ multiplets for Kr ions in the different charge states were calculated by means of the B-spline R-matrix code [57]. For each of the ionization steps the basis wave functions of the initial 9 and the final 17 states listed in Table I were obtained in the way described in [51], where one can also find the photoionization cross sections for each step and comparison with other theories and experiments for neutral krypton ionization. For all transitions except those involving $4s^0 4p^6$ and $4s^1 4p^6 1P$ states the difference of the calculated and NIST binding energies is below 0.6–0.8 eV, which corresponds to the detector resolution used in the paper.

Figure 2 illustrates the main idea of the paper: to account for the dynamical change of the polarization and its impact to the observable values. It shows alignment of the “first” ion $\text{Kr}^+ 4s^2 4p^5 2P$ as a function of time [Eq. (14)] and its stationary alignment [Eq. (15)]. The conventional alignment [Fig. 2(b)] as a function of energy has a broad maximum of absolute value caused by the Cooper minimum of the $4p \rightarrow \epsilon d$ ionization amplitude. At the Cooper minimum, alignment approaches to $-\sqrt{2}$, that is the minimal possible value al-

lowed by Eq. (17). One can see [Fig. 2(a)] that at the pulse beginning the alignment is equal to the conventional value at the corresponding photon energy: -0.5 ($\omega = 50$ eV), -1 ($\omega = 65$ eV), and -1.41 ($\omega = 80$ eV). Then as the linearly polarized pulse ionizes the ion preferably from $|m| = 1$, the alignment tends to amplify, and it is clearly seen for $\omega = 50$ and 65 eV. Moreover, originally smaller alignment at $\omega = 50$ eV may become stronger than at $\omega = 65$ eV due to the dynamical effects. At $\omega = 80$ eV the tendency is suppressed by the complete depletion of the $|m| = 1$ sublevels. Figure 3 shows stationary alignment [Eq. (15)] of the other ions assuming that they are created from an *unpolarized* state $\mathcal{A}_i = 0$. There are three types of features one can see: (i) the series of sharp structures at the lower-energy edge; (ii) broad deep minima or high maxima placed around $\omega = 70-80$ eV; and (iii) no energy dependency for some ionization pathways.

(i) The sharp structures emerge due to the Rydberg autoionization series and are observed in all spectra except ones corresponding to the highest allowed threshold, e.g., 1–3, 2–8, 3–9, {4, 5, 6}–16, and {7, 8, 9}–17. The resonance structure can hardly be resolved in the modern experiments and therefore it is not a subject of current investigation. Here we cut off most of the resonances, leaving a few just for an illustration.

(ii) The minima and maxima are connected with the Cooper minimum in $4p \rightarrow \epsilon d$ ionization amplitudes. Note that most of them are quite close to the allowed limits: $-\sqrt{2}$ and $1/\sqrt{2}$ for P terms [Eq. (17)] and $\pm\sqrt{7/10}$ for D terms [Eq. (18)].

(iii) Weak dependency on energy is explained by the domination of a particular channel. In order to explore the issue further, it is constructive to present Eq. (5) in a simpler form via single-electron transition amplitude d_{li} from l_i shell to ϵl continuum, i.e., neglecting term dependency of the amplitudes:

$$\begin{aligned} \bar{B}[k_i, k_\gamma, k_f] &= \hat{k}_i \hat{k}_\gamma (k_i 0, k_\gamma 0 | k_f 0) \hat{L}_i \hat{L}_f (-1)^{k_\gamma} \\ &\times \sum_l \left\{ \begin{matrix} 1 & 1 & k_\gamma \\ l_i & l_i & l \end{matrix} \right\} \left\{ \begin{matrix} l_i & L_i & L_f \\ l_i & L_i & L_f \\ k_\gamma & k_i & k_f \end{matrix} \right\} |d_{li}|^2. \end{aligned} \quad (21)$$

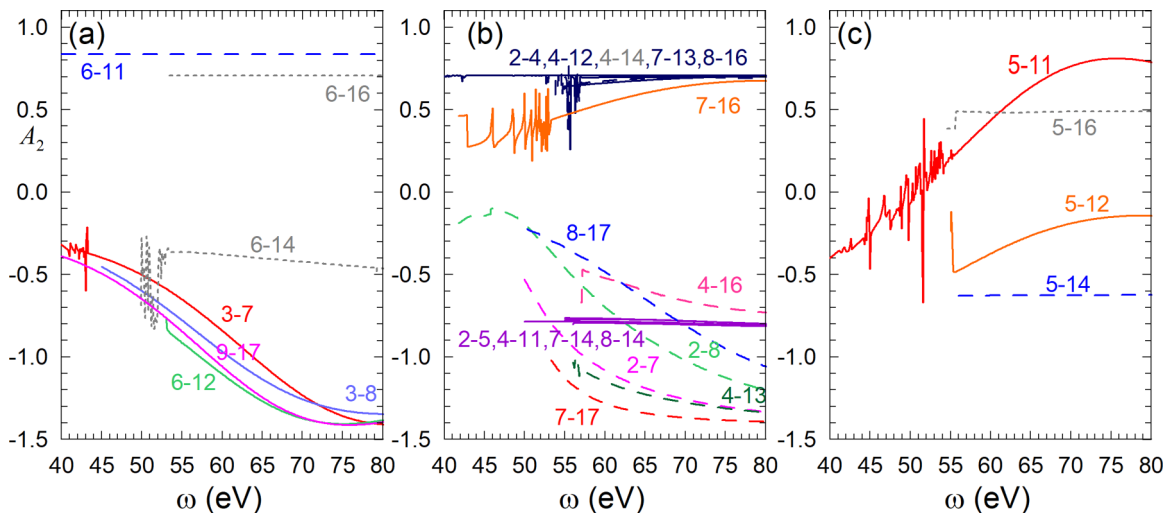


FIG. 3. The stationary alignment as a function of energy for the different ionization pathways: (a) from ions with the $4s^n 4p^m 2S_i+1 S$ term, (b) from the $4s^n 4p^m 2S_i+1 P$ term, and (c) from the $4s^n 4p^m 2S_i+1 D$ term.

We refer to this simplification as the *no correlations* (NC) model.

A. Ionization of the 4s shell

Within the NC model $L_i = L_f$ and the polarization of an initial state simply transfers to a final ion: $\mathcal{A}_f = \mathcal{A}_i$. That means that nonzero alignment of these branches (marked by dashed lines in Fig. 3) is a result of the correlation effects originating from strong term mixing. Moreover, branches 4–14, 4–15, 5–15, 5–16, 6–14, and 6–16 are not allowed in the simple NC model at all, because without correlations ionization of a s shell cannot change the term of an ion. Their cross sections are much lower than others [51]. Branch 6–16 is governed by Eqs. (5) and (15) and allowed due to the correlations single channel $\langle {}^2P\epsilon p^1P || \hat{D} || {}^1S \rangle$ which leads to $\mathcal{A}_f = 1/\sqrt{2}$.

B. Ionization of the 4p shell

Let us introduce $\kappa = |d_{pd}|^2/|d_{ps}|^2$ and rearrange Eqs. (15) using (21) as

$$\mathcal{A}_f = -\sqrt{2} \frac{1 + \frac{\kappa}{10}}{1 + \kappa}, \quad \begin{matrix} L_i=S \\ L_f=P, \end{matrix} \quad (22)$$

$$\mathcal{A}_f = \frac{\frac{1}{\sqrt{2}}(1 + \frac{\kappa}{10}) + \mathcal{A}_i(\frac{1}{2} - \frac{2}{5}\kappa)}{1 + \kappa + \mathcal{A}_i/\sqrt{2}(1 + \frac{\kappa}{10})}, \quad \begin{matrix} L_i=P \\ L_f=P, \end{matrix} \quad (23)$$

$$\mathcal{A}_f = -\sqrt{\frac{7}{10}} \frac{1 + \frac{\kappa}{10} - \mathcal{A}_i\sqrt{2}(\frac{5}{14} + \frac{17}{35}\kappa)}{1 + \kappa - \mathcal{A}_i\frac{\sqrt{2}}{10}(1 + \frac{\kappa}{10})}, \quad \begin{matrix} L_i=P \\ L_f=D. \end{matrix} \quad (24)$$

Equation (22) governs 1–2, 3–7, 3–8, 6–12, and 9–17 branches. They generally demonstrate essential energy dependence because of interplay between d_s and d_d amplitudes [see Fig. 3(a)]. Branch 6–11 is not allowed in the NC model, governed by Eqs. (5) and (15), hence the alignment determined by the only allowed channel $\langle {}^2D\epsilon d^1P || \hat{D} || {}^1S \rangle$ is $\mathcal{A}_f = \sqrt{7/10}$.

Equation (23) governs 2–4, 4–12, 7–13, 7–16, and 8–16 branches. All of them are practically independent of energy and very close to $\mathcal{A}_f = 1/\sqrt{2}$, indicating the domination of the s wave ($\kappa \approx 0$). The same is correct for 2–5 and 4–11 governed by Eq. (24): for them alignment values are close to $\mathcal{A}_f = -\sqrt{7/10}$.

In Fig. 3 all initial states are supposed to be unpolarized. *Ab initio* it is correct only for S terms [Fig. 3(a)]. Below we discuss how Figs. 3(b) and 3(c) are affected by the polarization of an initial state.

Equation (23) shows that while κ is small, P - P ionization causes the maximal possible positive alignment $\mathcal{A}_f = 1/\sqrt{2}$ independently of the alignment of an initial state. But the closer polarization of initial state \mathcal{A}_i to $-\sqrt{2}$, the lower s -wave contribution, finally at $\mathcal{A}_i = -\sqrt{2}$ s -wave contributions are completely compensated both in the numerator and denominator and the channel is closed. In this situation (as well as if the d wave dominates) alignment of the final state tends to the edge negative value $\mathcal{A}_f = -\sqrt{2}$.

Equation (24) shows that where the s wave dominates the alignment of a final state varies from $\mathcal{A}_f = -\sqrt{10/7}$ (minimal possible) at initial state $\mathcal{A}_i = -\sqrt{2}$ to twice smaller $\mathcal{A}_f = -\sqrt{5/14}$ at $\mathcal{A}_i = 1/\sqrt{2}$. At negative \mathcal{A}_i the d wave weakly

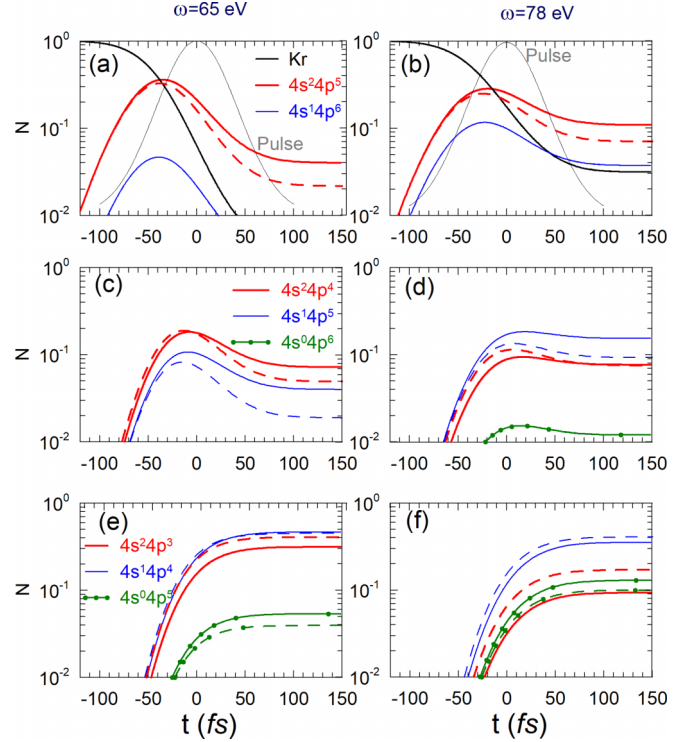


FIG. 4. Population of the different ion charge states and configurations for the fluence $F = 1000 \text{ ph}/\text{\AA}^2$ at the photon energies 65 eV (a), (c), (e) and 78 eV (b), (d), (f) calculated with (solid lines) and without (dashed lines) accounting for the polarization of the ionic states. The populations of the neutral Kr and Kr^+ are presented in the first row (a), (b); the population of Kr^{2+} is presented in the second row (c), (d). Black lines, yield of neutral Kr; thick red lines, yield of the ions with $4s^24p^{6-n}$ configuration, where n is the ion charge; thin blue lines, the ions with $4s^14p^{6-n+1}$ configuration; circled green lines, the ions with $4s^04p^{6-n+2}$ configuration. The third row (e), (f) presents populations of Kr^{3+} species provided that there is no next step; therefore circled green lines show the low limit for the species with double $4s$ vacancy in Kr^{3+} and higher states, and thick red lines show the upper limit for species without vacancy in the $4s$ shell in Kr^{3+} . The pulse envelope (gray line) is indicated in the upper panels. The missed green lines in panels (c) and (d) are below the plot region.

modifies the alignment because it works “to the same side” (the sign before κ is always positive). For example, at $\mathcal{A}_i = -\sqrt{2}$ the ratio between \mathcal{A}_f at $\kappa = 0$ (the s wave dominates) and \mathcal{A}_f at $\kappa \rightarrow \infty$ (the d wave dominates) is $25/22 \approx 1.14$.

From the above, one can see that while the NC model describes ionization from the valence $4p$ shell pretty well, it completely fails for the $4s$ shell, indicating much stronger correlations in ionization of the subvalence shell.

IV. RESULTS AND DISCUSSION

In this section we present and discuss results for the observable values: population of the different ionic species (Fig. 4), ionic yields (Fig. 5), and photoelectron spectra (Fig. 6). As was discussed in [51], the curves in Figs. 4–6 remain the same for a fixed value of fluence F if we change the pulse duration and do the appropriate scaling of the timescale. The reason for

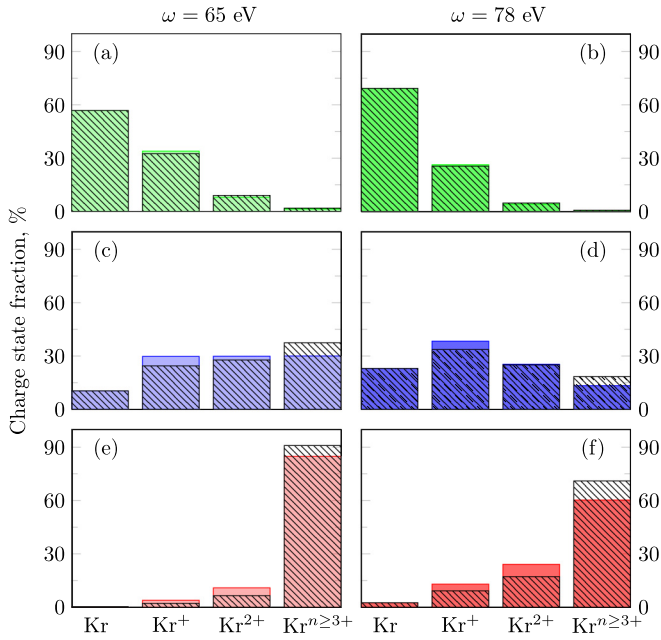


FIG. 5. The charge-state yields for three fluences: $F = 100$ $\text{ph}/\text{\AA}^2$ (a), (b), $F = 400$ $\text{ph}/\text{\AA}^2$ (c), (d), and $F = 1000$ $\text{ph}/\text{\AA}^2$ (e), (f) for the photon energies 65 eV (a), (c), (e) and 78 eV (b), (d), (f). The shaded areas show the results for unpolarized radiation.

the scaling is absence of any natural timetick (like the Auger decay) in the system under consideration.

A. The ionic yields

In Fig. 4 we present results for the linearly polarized and unpolarized radiation at two photon energies (65 and 78 eV, in order to stay below the hidden resonance) and the fluence $F = 1000$ $\text{ph}/\text{\AA}^2$ corresponding to intensity 2.2×10^{15} W/cm^2 (at $t_p = 60$ fs). We present population as a function of time summed up within one configuration over possible terms.

The concentration of neutral atoms monotonically decreases with time [Figs. 4(a) and 4(b)]. The number of singly and doubly charged ions first increases with time, but then it may drop down [Figs. 4(c) and 4(d)], because of their further ionization to Kr^{3+} . At any time the sum of all populations presented in Fig. 4 corresponding to the same fluence, photon energy, and polarization equals unity.

At the first step [Figs. 4(a) and 4(b)] the alignment of the $\text{Kr}^+ 4s^2 4p^5 {}^2P$ ion prevents its further ionization triply increasing its final population (thick red curves). In the low intensity regime this tendency would keep: polarization of an ion simply suppresses some of the ionization channels, leaving the other channels unaffected. If intensity is high enough to involve the saturation and depletion effects the tendency is violated. For example, accounting for the alignment increases the number of double $4s$ -hole $\text{Kr}^{2+} 4s^0 4p^6 {}^1S$ ions [circled green lines in Fig. 4(c)] in spite of the fact that the ions are created in the pathway affecting only S terms. The tendency is also relevant for the next step [Fig. 4(e)]. For photon energy $\omega = 78$ eV corresponding to higher alignment of Kr^+ the polarization rearranges ionic yields: for unpolarized radiation output of $4s^2 4p^3$ is higher than $4s^0 4p^5$, while for polarized

radiation output of $4s^0 4p^5$ is higher [thick red and circled green lines in Fig. 4(f)].

Such a high yield of $4s$ single- and double-hole ions at $\omega = 65$ eV is really surprising considering that there are Cooper minima in $4s$ -shell ionization of both Kr and Kr^+ [51] situated in the region of 45–50 eV and, moreover, including the fact that the $4s$ -ionization cross section at $\omega = 65$ eV is still one order of magnitude lower than the $4p$ -ionization cross section.

Cross sections of the $4p$ -shell ionization in both atom and ions are lower at $\omega = 78$ eV than at $\omega = 65$ eV due to closeness of the Cooper minima. As a result, the summed yield of the double $4s$ -hole states ($0.012 + 0.13$) is higher than for 65 eV ($0.0006 + 0.054$); the summed yield of the single $4s$ -hole states ($0.037 + 0.15 + 0.35$) is practically equal ($0.004 + 0.04 + 0.47$). Note that possible next photoionization steps which are not included in the current consideration may only increase the overall number of double $4s$ vacancies. Results for the $\text{Kr}^+ 4s^2 4p^5$ ion may look contradicted: in spite of the cross section dropping down by a factor of 3, the yield increases by a factor of 5 between 65 and 78 eV [red lines in Figs. 4(a) and 4(b)]. That is because very high (minimal) alignment prohibits the next ionization step, causing the ion accumulation.

In practice the different ionic configurations are not distinguished. In Fig. 5, the overall ionic yields at the fluences $F = 100$, 400, and 1000 $\text{ph}/\text{\AA}^2$ and the photon energies $\omega = 65$ and 78 eV are presented. The relative populations of the different ionic states change with intensity, switching from the perturbative [Figs. 5(a) and 5(b)] to the saturation [Figs. 5(e) and 5(f)] patterns. As expected, summing over the configurations decreases difference between polarized and unpolarized cases. At lower intensity [Figs. 5(a) and 5(b)] there are no polarization effects, but at higher ones they become more essential and may keep up to 10% of the total ionic number of ions in low charge states Kr^+ and Kr^{2+} [Figs. 5(c) and 5(f)].

The next step, i.e., the ionization of Kr^{3+} by 78 eV photons, is energetically possible and the last column in Figs. 5(b), 5(e) and 5(f) presents the summed yield of ions with charges 3 and higher. Nevertheless, that cannot affect the presented below photoelectron spectra because it would contribute at higher binding energy.

B. Photoelectron spectra

The photoelectron spectrum can be cast as a function of the probability $P_{ab}(F)$ of an ion (atom) in a state a to be ionized into the ion in a state b over the entire pulse and of the energy of this transition:

$$f_F(\varepsilon) = \sum_{ab} P_{ab}(F) \exp[-(\varepsilon + I_{ab} - \omega)^2 / \Gamma^2], \quad (25)$$

where ε is the photoelectron kinetic energy, I_{ab} is the binding energy of ionization of the state a to the state b , and Γ is the resolution of the electron detector. As in [51], we set value $\Gamma = 0.42$ eV to leave the fine structure of levels unresolved.

The photoelectron spectrum provides more detailed information on the pathways of the sequential ionization than the ion yield because it ‘remembers’ the relative population of the intermediate states of the process (see Fig. 1 and Table I).

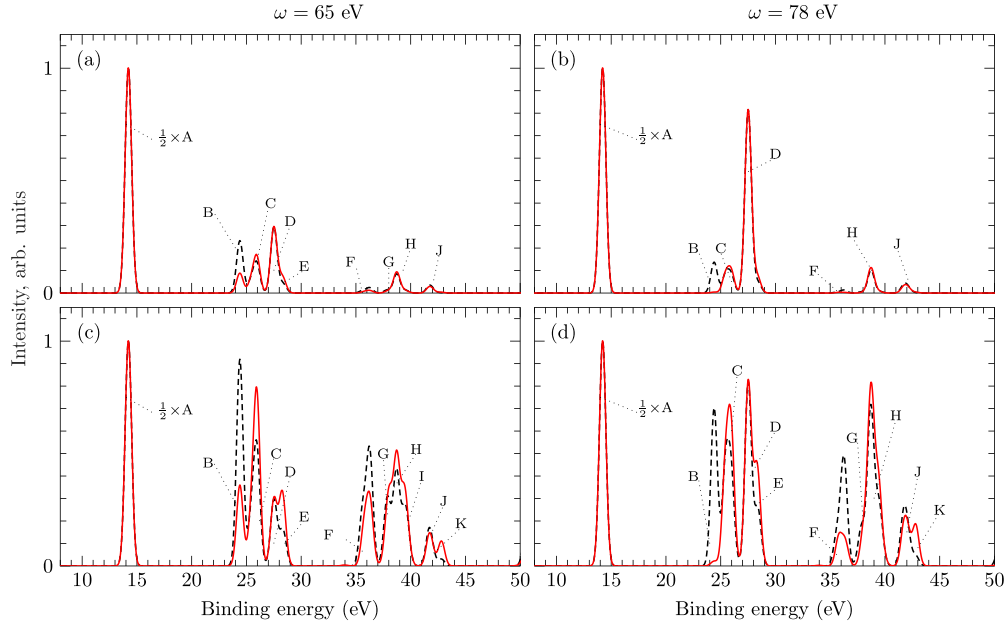


FIG. 6. Photoelectron spectrum for different photon energies: $\omega = 65$ eV [(a) for $F = 100$ ph/Å² and (c) for $F = 1000$ ph/Å²] and $\omega = 78$ eV [(b) for $F = 100$ ph/Å² and (d) for $F = 1000$ ph/Å²]. The solid lines correspond to calculations for linearly polarized radiation; the dashed lines correspond to unpolarized radiation. The spectra are normalized in such a way that $1/2$ of the main line A equals unity. The spectral features are indicated by capital letters in accordance with Table I. The difference of peak E for the dashed line compared to the data presented in [51] is because of the corrected cross section of the (2-6) channel.

The generated photoelectron spectra for two photon energies, 65 and 78 eV, are displayed in Figs. 6(a) and 6(c) and Figs. 6(b) and 6(d), correspondingly. We consider two values of fluence: low $F = 100$ ph/Å² [Figs. 6(a) and 6(b)] and high $F = 1000$ ph/Å² [Figs. 6(c) and 6(d)]. The dashed lines show the results obtained for unpolarized radiation.

In Figs. 6(a)–6(d) the lines are concentrated in three groups: the main photoline A from the $4p$ -shell ionization of neutral Kr, the lines from ionization of $\text{Kr}^+ 4s^2 4p^5$ mostly (B–E), and the lines from ionization of $\text{Kr}^{2+} 4s^2 4p^4$ mostly (F–K).

For the low-intensity regime [Fig. 6(a)] the polarization suppresses line B and completely demolishes it at $\omega = 78$ eV [Fig. 6(b)]. That is because $\text{Kr}^+ 4s^2 4p^5 2P$ is completely polarized ($A_2(P) = -\sqrt{2}$) in the region of the Cooper minimum and the polarization does not allow ionization to the s wave (rule 23). Line F demonstrates similar behavior, but at the considered intensity regime it is difficult to see.

The case of higher fluence [Figs. 6(c) and 6(d)] is more interesting. Besides overall increasing of the multiple ionization contributions which appears in enlarging peaks for the binding energy above 30 eV and decreasing above discussed lines B and F, there are some lines which increase or even appear in comparison with the unpolarized case. These are line E, which can be distinguished only for polarized radiation, and line K. The redistribution is caused by the enhanced contributions from ionization of S terms, while the ionization of P terms is suppressed by the polarization.

Figure 7 shows the fluence dependence of the intensities of the spectral lines P_{ab} contributing at the same energy. The curves clearly indicate the one-, two-, and three-photon origin of the spectral features A, (B and C), and (F and G), respectively. The lines incorporating the contributions of different

processes (for example, peak G) behave transiently. The saturation appears at fluence above 100 ph/Å². The figure shows

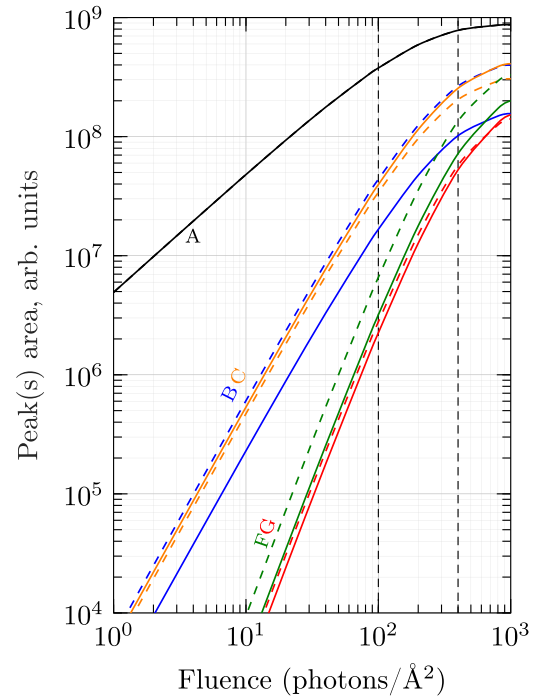


FIG. 7. Intensity dependence of the different photoelectron lines on the fluence F at the photon energy $\omega = 65$ eV. The vertical dashed lines indicate fluences related to Figs. 4–6: 100 and 400 ph/Å². The solid lines correspond to linear polarization of the field; the dashed lines correspond to the unpolarized radiation.

that accounting for the polarization does not change general multiphoton behavior with intensity.

V. CONCLUSION

The role of the polarization of both radiation and ionic states in sequential multiple ionization is studied theoretically. The system of equations similar to the conventional rate equations for states population is formulated in terms of the statistical tensors of angular momentum. It is applicable to linearly and circularly polarized pulses irradiating a system with well-separated (excited incoherently) levels within the dipole approximation.

The method is applied to multiple ionization of Kr in the 65–80-eV region. The method was tested for the conditions providing extreme, i.e., maximal positive or minimal negative, alignment. Analysis of the high intensity regime has shown that high-rank $k \geq 4$ is crucially important for the system consistency and cannot be considered as a perturbation. The ionic states evolution, the yields, and the photoelectron spectra are calculated and compared for the linearly polarized and the unpolarized radiation. Redistribution of the ionic yields up to 10% of total amount and noticeable rearrangement of the photoelectron spectrum caused by polarization are predicted. In the low-intensity regime the polarization works as a damper suppressing or even demolishing some photolines; in the high-intensity regime the polarization works as a trigger emphasizing structures of the spectrum. Some lines become distinguishable only for the polarized radiation.

It is shown that the doubly hollow ionic states which can decay only via spontaneous emission are created more efficiently if a sample is irradiated by the linearly polarized radiation than by the unpolarized one. These hollow ion states are of particular interest because they can serve as a target to create autoionizing states of a very exotic configuration.

The discussed effects are expected to be more significant for the circularly polarized radiation. Moreover, conjugate measurements with linearly and circularly polarized pulses will allow one to distinguish the effect in the ionic yields more clearly. The effects are expected to appear if a spectroscopic feature causing a strong modulation of the polarization (a resonance excitation, an autoionizing state, or the Cooper minimum) takes place at an early ionization step. For example, the present paper is a necessary point before studying the complex evolution of the system due to different opening Auger decay channels which become possible when the 3d-shell ionization comes into play.

ACKNOWLEDGMENTS

The research was funded by the Russian Foundation for Basic Research under Project No. 20-52-12023 and Ministry of Science and Higher Education of the Russian Federation Grant No. 075-15-2021-1353. The work of M.D.K. is supported by the Ministry of Science and Higher Education of the Russian Federation (Project No. 0818-2020-0005) using resources of the Shared Services “Data Center of the Far-Eastern Branch of the Russian Academy of Sciences.”

-
- [1] L. Budewig, S.-K. Son, and R. Santra, Theoretical investigation of orbital alignment of x-ray-ionized atoms in exotic electronic configurations, *Phys. Rev. A* **105**, 033111 (2022).
- [2] E. Heinrich-Josties, S. Pabst, and R. Santra, Controlling the 2p hole alignment in neon via the 2s-3p Fano resonance, *Phys. Rev. A* **89**, 043415 (2014).
- [3] K. Nass, L. Foucar, T. R. M. Barends, E. Hartmann, S. Botha, R. L. Shoeman, R. B. Doak, R. Alonso-Mori, A. Aquila, S. Bajt, A. Barty, R. Bean, K. R. Beyerlein, M. Bublitz, N. Drachmann, J. Gregersen, H. O. Jonsson, W. Kabsch, S. Kassemeyer, J. E. Koglin *et al.*, Indications of radiation damage in ferredoxin microcrystals using high-intensity X-FEL beams, *J. Synchrotron Radiat.* **22**, 225 (2015).
- [4] L. Galli, S.-K. Son, M. Klinge, S. Bajt, A. Barty, R. Bean, C. Betzel, K. R. Beyerlein, C. Caleman, R. B. Doak, M. Duszenko, H. Fleckenstein, C. Gati, B. Hunt, R. A. Kirian, M. Liang, M. H. Nanao, K. Nass, D. Oberthur, L. Redecke *et al.*, Electronic damage in s atoms in a native protein crystal induced by an intense x-ray free-electron laser pulse, *Struct. Dyn.* **2**, 041703 (2015).
- [5] A. A. Sorokin, S. V. Bobashev, T. Feigl, K. Tiedtke, H. Wabnitz, and M. Richter, Photoelectric Effect at Ultrahigh Intensities, *Phys. Rev. Lett.* **99**, 213002 (2007).
- [6] M. Kübel, C. Burger, N. G. Kling, T. Pischke, L. Beaufore, I. Ben-Itzhak, G. G. Paulus, J. Ullrich, T. Pfeifer, R. Moshhammer, M. F. Kling, and B. Bergues, Complete characterization of single-cycle double ionization of argon from the nonsequential to the sequential ionization regime, *Phys. Rev. A* **93**, 053422 (2016).
- [7] R. Moshhammer, Y. H. Jiang, L. Foucar, A. Rudenko, T. Ergler, C. D. Schröter, S. Lüdemann, K. Zrost, D. Fischer, J. Titze, T. Jahnke, M. Schöffler, T. Weber, R. Dörner, T. J. M. Zouros, A. Dorn, T. Ferger, K. U. Kühnel, S. Düsterer, R. Treusch *et al.*, Few-Photon Multiple Ionization of Ne and Ar by Strong Free-Electron-Laser Pulses, *Phys. Rev. Lett.* **98**, 203001 (2007).
- [8] M. Fushitani, Y. Sasaki, A. Matsuda, H. Fujise, Y. Kawabe, K. Hashigaya, S. Owada, T. Togashi, K. Nakajima, M. Yabashi, Y. Hikosaka, and A. Hishikawa, Multielectron-Ion Coincidence Spectroscopy of Xe in Extreme Ultraviolet Laser Fields: Non-linear Multiple Ionization via Double Core-Hole States, *Phys. Rev. Lett.* **124**, 193201 (2020).
- [9] L. Young, E. P. Kanter, B. Krässig, Y. Li, A. M. March, S. T. Pratt, R. Santra, S. H. Southworth, N. Rohringer, L. F. DiMauro, G. Doumy, C. A. Roedig, N. Berrah, L. Fang, M. Hoener, P. H. Bucksbaum, J. P. Cryan, S. Ghimire, J. M. Glowia, D. A. Reis *et al.*, Femtosecond electronic response of atoms to ultra-intense X-rays, *Nature (London)* **466**, 56 (2010).
- [10] E. P. Kanter, B. Krässig, Y. Li, A. M. March, P. Ho, N. Rohringer, R. Santra, S. H. Southworth, L. F. DiMauro, G. Doumy, C. A. Roedig, N. Berrah, L. Fang, M. Hoener, P. H. Bucksbaum, S. Ghimire, D. A. Reis, J. D. Bozek, C. Bostedt, M. Messerschmidt *et al.*, Unveiling and Driving Hidden

- Resonances with High-Fluence, High-Intensity X-Ray Pulses, *Phys. Rev. Lett.* **107**, 233001 (2011).
- [11] S. Klumpp, N. Gerken, K. Mertens, M. Richter, B. Sonntag, A. A. Sorokin, M. Braune, K. Tiedtke, P. Zimmermann, and M. Martins, Multiple Auger cycle photoionisation of manganese atoms by short soft x-ray pulses, *New J. Phys.* **19**, 043002 (2017).
- [12] N. Berrah, L. Fang, T. Osipov, B. Murphy, C. Bostedt, and J. Bozek, Multiphoton ionization and fragmentation of molecules with the LCLS x-ray FEL, *J. Electron Spectrosc. Relat. Phenom.* **196**, 34 (2014).
- [13] H. Fukuzawa, S.-K. Son, K. Motomura, S. Mondal, K. Nagaya, S. Wada, X.-J. Liu, R. Feifel, T. Tachibana, Y. Ito, M. Kimura, T. Sakai, K. Matsunami, H. Hayashita, J. Kajikawa, P. Johnsson, M. Siano, E. Kukk, B. Rudek, B. Erk *et al.*, Deep Inner-Shell Multiphoton Ionization by Intense X-Ray Free-Electron Laser Pulses, *Phys. Rev. Lett.* **110**, 173005 (2013).
- [14] S. H. Southworth, R. W. Dunford, D. Ray, E. P. Kanter, G. Doumy, A. M. March, P. J. Ho, B. Krässig, Y. Gao, C. S. Lehmann, A. Picon, L. Young, D. A. Walko, and L. Cheng, Observing pre-edge k-shell resonances in Kr, Xe, and XeF₂, *Phys. Rev. A* **100**, 022507 (2019).
- [15] M. Kurka, A. Rudenko, L. Foucar, K. U. Kühnel, Y. H. Jiang, T. Ergler, T. Havermeier, M. Smolarski, S. Schössler, K. Cole, M. Schöffler, R. Dörner, M. Gensch, S. Düsterer, R. Treusch, S. Fritzsche, A. N. Grum-Grzhimailo, E. V. Gryzlova, N. M. Kabachnik, C. D. Schröter *et al.*, Two-photon double ionization of Ne by free-electron laser radiation: A kinematically complete experiment, *J. Phys. B: At. Mol. Opt. Phys.* **42**, 141002 (2009).
- [16] M. Braune, G. Hartmann, M. Ilchen, A. Knie, T. Lischke, A. Reinköster, A. Meissner, S. Deinert, L. Glaser, O. Al-Dossary, A. Ehresmann, A. S. Kheifets, and J. Viehhaus, Electron angular distributions of noble gases in sequential two-photon double ionization, *J. Mod. Opt.* **63**, 324 (2016).
- [17] P. A. Carpeggiani, E. V. Gryzlova, M. Reduzzi, A. Dubrouil, D. Faccialá, M. Negro, K. Ueda, S. M. Burkov, F. Frassetto, F. Stienkemeier, Y. Ovcharenko, M. Meyer, O. Plekan, P. Finetti, K. C. Prince, C. Callegari, A. N. Grum-Grzhimailo, and G. Sansone, Complete reconstruction of bound and unbound electronic wave functions in two-photon double ionization, *Nat. Phys.* **15**, 170 (2019).
- [18] T. Mazza, M. Ilchen, M. D. Kiselev, E. V. Gryzlova, T. M. Baumann, R. Boll, A. De Fanis, P. Grychtol, J. Montaño, V. Music, Y. Ovcharenko, N. Rennhack, D. E. Rivas, P. Schmidt, R. Wagner, P. Ziolkowski, N. Berrah, B. Erk, P. Johnsson, C. Küstner-Wetekam *et al.*, Mapping Resonance Structures in Transient Core-Ionized Atoms, *Phys. Rev. X* **10**, 041056 (2020).
- [19] N. Gerken, S. Klumpp, A. A. Sorokin, K. Tiedtke, M. Richter, V. Bürk, K. Mertens, P. Juranić, and M. Martins, Time-Dependent Multiphoton Ionization of Xenon in the Soft-X-Ray Regime, *Phys. Rev. Lett.* **112**, 213002 (2014).
- [20] M. Richter, S. V. Bobashev, A. A. Sorokin, and K. Tiedtke, Multiphoton ionization of atoms with soft x-ray pulses, *J. Phys. B: At. Mol. Opt. Phys.* **43**, 194005 (2010).
- [21] G. Doumy, C. Roedig, S.-K. Son, C. I. Blaga, A. D. DiChiara, R. Santra, N. Berrah, C. Bostedt, J. D. Bozek, P. H. Bucksbaum, J. P. Cryan, L. Fang, S. Ghimire, J. M. Glowina, M. Hoener, E. P. Kanter, B. Krässig, M. Kuebel, M. Messerschmidt, G. G. Paulus *et al.*, Nonlinear Atomic Response to Intense Ultrashort X Rays, *Phys. Rev. Lett.* **106**, 083002 (2011).
- [22] E. Allaria, B. Diviacco, C. Callegari, P. Finetti, B. Mahieu, J. Viehhaus, M. Zangrando, G. De Ninno, G. Lambert, E. Ferrari, J. Buck, M. Ilchen, B. Vodungbo, N. Mahne, C. Svetina, C. Spezzani, S. Di Mitri, G. Penco, M. Trovó, W. M. Fawley *et al.*, Control of the Polarization of a Vacuum-Ultraviolet, High-Gain, Free-Electron Laser, *Phys. Rev. X* **4**, 041040 (2014).
- [23] T. Mazza *et al.*, Determining the polarization state of an extreme ultraviolet free-electron laser beam using atomic circular dichroism, *Nat. Commun.* **5**, 3648 (2014).
- [24] A. A. Lutman *et al.*, Polarization control in an x-ray free-electron laser, *Nat. Photon.* **10**, 468 (2016).
- [25] A. S. Kheifets, Sequential two-photon double ionization of noble gas atoms, *J. Phys. B: At. Mol. Opt. Phys.* **40**, F313 (2007).
- [26] A. N. Grum-Grzhimailo, E. V. Gryzlova, S. Fritzsche, and N. M. Kabachnik, Photoelectron angular distributions and correlations in sequential double and triple atomic ionization by free electron lasers, *J. Mod. Opt.* **63**, 334 (2016).
- [27] S. Mondal, R. Ma, K. Motomura, H. Fukuzawa, A. Yamada, K. Nagaya, S. Yase, Y. Mizoguchi, M. Yao, A. Rouzée, A. Hundertmark, M. J. J. Vrakking, P. Johnsson, M. Nagasono, K. Tono, T. Togashi, Y. Senba, H. Ohashi, M. Yabashi, T. Ishikawa *et al.*, Photoelectron angular distributions for the two-photon sequential double ionization of xenon by ultrashort extreme ultraviolet free electron laser pulses, *J. Phys. B: At. Mol. Opt. Phys.* **46**, 164022 (2013).
- [28] M. Ilchen, G. Hartmann, E. V. Gryzlova, A. Achner, E. Allaria, A. Beckmann, M. Braune, J. Buck, C. Callegari, R. N. Coffee, R. Cucini, M. Danailov, A. De Fanis, A. Demidovich, E. Ferrari, P. Finetti, L. Glaser, A. Knie, A. O. Lindahl, O. Plekan *et al.*, Symmetry breakdown of electron emission in extreme ultraviolet photoionization of argon, *Nat. Commun.* **9**, 4659 (2018).
- [29] S. Augustin, M. Schulz, G. Schmid, K. Schnorr, E. V. Gryzlova, H. Lindenblatt, S. Meister, Y. F. Liu, F. Trost, L. Fechner, A. N. Grum-Grzhimailo, S. M. Burkov, M. Braune, R. Treusch, M. Gisselbrecht, C. D. Schröter, T. Pfeifer, and R. Moshhammer, Signatures of autoionization in the angular electron distribution in two-photon double ionization of Ar, *Phys. Rev. A* **98**, 033408 (2018).
- [30] A. Rouzee, P. Johnsson, E. V. Gryzlova, H. Fukuzawa, A. Yamada, W. Siu, Y. Huismans, E. Louis, F. Bijkerk, D. M. P. Holland, A. N. Grum-Grzhimailo, N. M. Kabachnik, M. J. J. Vrakking, and K. Ueda, Angle-resolved photoelectron spectroscopy of sequential three-photon triple ionization of neon at 90.5 eV photon energy, *Phys. Rev. A* **83**, 031401(R) (2011).
- [31] N. M. Kabachnik, S. Fritzsche, A. N. Grum-Grzhimailo, M. Meyer, and K. Ueda, Coherence and correlations in photoinduced Auger and fluorescence cascades in atoms, *Phys. Rep.* **451**, 155 (2007).
- [32] P. O’Keeffe, E. V. Gryzlova, D. Cubaynes, G. A. Garcia, L. Nahon, A. N. Grum-Grzhimailo, and M. Meyer, Isotopically Resolved Photoelectron Imaging Unravels Complex Atomic Autoionization Dynamics by Two-Color Resonant Ionization, *Phys. Rev. Lett.* **111**, 243002 (2013).
- [33] P. Wernet, J. Schulz, B. Sonntag, K. Godehusen, P. Zimmermann, A. N. Grum-Grzhimailo, N. M. Kabachnik, and M. Martins, *2p* photoelectron spectra and linear

- alignment dichroism of atomic Cr, *Phys. Rev. A* **64**, 042707 (2001).
- [34] M. Meyer, A. N. Grum-Grzhimailo, D. Cubaynes, Z. Felfli, E. Heinecke, S. T. Manson, and P. Zimmermann, Magnetic Dichroism in *k*-Shell Photoemission from Laser Excited Li Atoms, *Phys. Rev. Lett.* **107**, 213001 (2011).
- [35] M. Wedowski, K. Godehusen, F. Weisbarth, P. Zimmermann, M. Martins, T. Dohrmann, A. von dem Borne, B. Sonntag, and A. N. Grum-Grzhimailo, Vacuum-ultraviolet photoelectron spectroscopy of laser-excited aligned Ca atoms in the 3p-3d resonance region, *Phys. Rev. A* **55**, 1922 (1997).
- [36] M. Ilchen, N. Douguet, T. Mazza, A. J. Rafipoor, C. Callegari, P. Finetti, O. Plekan, K. C. Prince, A. Demidovich, C. Grazioli, L. Avaldi, P. Bolognesi, M. Coreno, M. Di Fraia, M. Devetta, Y. Ovcharenko, S. Düsterer, K. Ueda, K. Bartschat, A. N. Grum-Grzhimailo *et al.*, Circular Dichroism in Multiphoton Ionization of Resonantly Excited He⁺ Ions, *Phys. Rev. Lett.* **118**, 013002 (2017).
- [37] D. Cubaynes, M. Meyer, A. N. Grum-Grzhimailo, J.-M. Bizau, E. T. Kennedy, J. Bozek, M. Martins, S. Canton, B. Rude, N. Berrah, and F. J. Wuilleumier, Dynamically and Quasiforbidden Transitions in Photoionization of Open-Shell Atoms: A Combined Experimental and Theoretical Study, *Phys. Rev. Lett.* **92**, 233002 (2004).
- [38] W. Nörtershäuser, A. Surzhykov, R. Sánchez, B. Botermann, G. Gwinner, G. Huber, S. Karpuk, T. Kühl, C. Novotny, S. Reinhardt, G. Saathoff, T. Stöhlker, and A. Wolf, Polarization-dependent disappearance of a resonance signal: Indication for optical pumping in a storage ring? *Phys. Rev. Accel. Beams* **24**, 024701 (2021).
- [39] E. T. Karamatskos, D. Markellos, and P. Lambropoulos, Multiple ionization of argon under 123 eV FEL radiation and the creation of 3s-hollow ions, *J. Phys. B: At. Mol. Opt. Phys.* **46**, 164011 (2013).
- [40] T. Nakajima and L. A. A. Nikolopoulos, Use of helium double ionization for autocorrelation of an XUV pulse, *Phys. Rev. A* **66**, 041402(R) (2002).
- [41] M. G. Makris, P. Lambropoulos, and A. Mihelič, Theory of Multiphoton Multielectron Ionization of Xenon under Strong 93-eV Radiation, *Phys. Rev. Lett.* **102**, 033002 (2009).
- [42] S.-K. Son, L. Young, and R. Santra, Impact of hollow-atom formation on coherent x-ray scattering at high intensity, *Phys. Rev. A* **83**, 033402 (2011).
- [43] S.-K. Son and R. Santra, Monte Carlo calculation of ion, electron, and photon spectra of xenon atoms in x-ray free-electron laser pulses, *Phys. Rev. A* **85**, 063415 (2012).
- [44] U. Lorenz, N. M. Kabachnik, E. Weckert, and I. A. Vartanyants, Impact of ultrafast electronic damage in single-particle x-ray imaging experiments, *Phys. Rev. E* **86**, 051911 (2012).
- [45] V. Y. Lunin, A. N. Grum-Grzhimailo, E. V. Gryzlova, D. O. Sinitsyn, T. E. Petrova, N. L. Lunina, N. K. Balabaev, K. B. Tereshkina, A. S. Stepanov, and Y. F. Krupyanskii, Efficient calculation of diffracted intensities in the case of nonstationary scattering by biological macromolecules under XFEL pulses, *Acta Crystallogr. D* **71**, 293 (2015).
- [46] S. Serkez, G. Geloni, S. Tomin, G. Feng, E. V. Gryzlova, A. N. Grum-Grzhimailo, and M. Meyer, Overview of options for generating high-brightness attosecond x-ray pulses at free-electron lasers and applications at the European XFEL, *J. Opt.* **20**, 024005 (2018).
- [47] C. Buth, R. Beerwerth, R. Obaid, N. Berrah, L. S. Cederbaum, and S. Fritzsche, Neon in ultrashort and intense x-rays from free electron lasers, *J. Phys. B: At. Mol. Opt. Phys.* **51**, 055602 (2018).
- [48] G. C. King, M. Tronc, F. H. Read, and R. C. Bradford, An investigation of the structure near the $l_{2,3}$ edges of argon, the $m_{4,5}$ edges of krypton and the $n_{4,5}$ edges of xenon, using electron impact with high resolution, *J. Phys. B: At. Mol. Phys.* **10**, 2479 (1977).
- [49] S. Svensson, B. Eriksson, N. Mårtensson, G. Wendin, and U. Gelius, Electron shake-up and correlation satellites and continuum shake-off distributions in x-ray photoelectron spectra of the rare gas atoms, *J. Electron Spectrosc. Relat. Phenom.* **47**, 327 (1988).
- [50] M. Ilchen, T. Mazza, E. T. Karamatskos, D. Markellos, S. Bakhtiarzadeh, A. J. Rafipoor, T. J. Kelly, N. Walsh, J. T. Costello, P. O’Keeffe, N. Gerken, M. Martins, P. Lambropoulos, and M. Meyer, Two-electron processes in multiple ionization under strong soft-x-ray radiation, *Phys. Rev. A* **94**, 013413 (2016).
- [51] E. V. Gryzlova, M. D. Kiselev, M. M. Popova, A. A. Zubekhin, G. Sansone, and A. N. Grum-Grzhimailo, Multiple sequential ionization of valence $n = 4$ shell of krypton by intense femtosecond XUV pulses, *Atoms* **8**, 80 (2020).
- [52] NIST Atomic Spectra Database (version 5.8) (National Institute of Standards and Technology, Gaithersburg, MD, 2020), <https://physics.nist.gov/asd> [May 18 2020].
- [53] V. V. Balashov, A. N. Grum-Grzhimailo, and M. Kabachnik, *Polarization and Correlation Phenomena in Atomic Collisions: A Practical Theory Course* (Plenum, New York, 2000).
- [54] K. Blum, *Density Matrix Theory and Applications* (Plenum, New York, 1996).
- [55] E. Allaria, R. Appio, L. Badano, W. A. Barletta, S. Bassanese, S. G. Biedron, A. Borga, E. Busetto, D. Castronovo, P. Cinquegrana, S. Cleva, D. Cocco, M. Cornacchia, P. Craievich, I. Cudin, G. D’Auria, M. Dal Forno, M. B. Danailov, R. De Monte, G. De Ninno *et al.*, Highly coherent and stable pulses from the FERMI seeded free-electron laser in the extreme ultraviolet, *Nat. Photonics* **6**, 699 (2012).
- [56] P. Finetti, H. Höppner, E. Allaria, C. Callegari, F. Capotondi, P. Cinquegrana, M. Coreno, R. Cucini, M. B. Danailov, A. Demidovich, G. De Ninno, M. Di Fraia, R. Feifel, E. Ferrari, L. Fröhlich, D. Gauthier, T. Goltz, C. Grazioli, Y. Kai, G. Kurdi *et al.*, Pulse Duration of Seeded Free-Electron Lasers, *Phys. Rev. X* **7**, 021043 (2017).
- [57] O. Zatsarinny, BSR: B-spline atomic R-matrix codes, *Comput. Phys. Commun.* **174**, 273 (2006).
- [58] U. Kleiman and B. Lohmann, Photoionization of closed-shell atoms: Hartree-Fock calculations of orientation and alignment, *J. Electron Spectrosc. Relat. Phenom.* **131-132**, 29 (2003).
- [59] E. Andersson, P. Linusson, S. Fritzsche, L. Hedin, J. H. D. Eland, L. Karlsson, J.-E. Rubensson, and R. Feifel, Formation of Kr³⁺ via core-valence doubly ionized intermediate states, *Phys. Rev. A* **85**, 032502 (2012).